Astronomy & Astrophysics manuscript no. output
November 26, 2025

Cosmic Expansion History from SNe Ia via Geometric Variational Inference - the charm2 code

Iason Saganas[1,2], Natalia Porqueres[3], Matteo Guardiani[2] and Torsten Enßlin[2]

[1] Ludwig-Maximilians-University Munich, Scheinerstr. 1, 81679 Munich, Germany
e-mail: I.Saganas@campus.lmu.de
[2] Max-Planck-Institute of Astrophysics, Karl-Schwarzschildstr. 1, 85748 Garching, Germany.
[3] Université Paris-Saclay, Université Paris Cité, CEA, CNRS, AIM, 91191, Gif-sur-Yvette, France

Received here; accepted then

ABSTRACT

Context. Cosmological analyses using the latest set of type Ia Supernova data favour an evolving dark energy model, challenging the standard ΛCDM cosmological paradigm. Non-parametric reconstructions of the expansion history help to examine the assumptions we impose on data by, e.g., uncovering signal features a parametric model might miss. Information Field Theory (IFT) is a Bayesian framework for optimal, non-parametric reconstruction algorithms.
Aims. In this work, we present charm2, the successor to charm1, a previous IFT-based code to reconstruct the cosmic energy density's redshift evolution from Supernovae Ia. We employ a model that strongly mitigates prior cosmological biases. We apply our reconstruction algorithm to the Union2.1, Pantheon+, and the DESY5 data set, to investigate the agreement between the non-parametric reconstruction and the signal suggested by a parametric, flat ΛCDM model.
Methods. We employ the novel geometric variational inference method that finds a coordinate transformation through which a potentially highly curved posterior distribution can be "flattened out" and thus be well approximated by a Gaussian distribution. Through the use of the "Correlated Field Model", we construct a Bayesian hierarchical model, able to infer central cosmological and statistical aspects of the signal. A slight reformulation of the instrument response compared to the charm1 predecessor permits us to evade the assumption of a fiducial value for H_0.
Results. The Union2.1 and Pantheon+ datasets are consistent with parametric flat ΛCDM signal fields, although in both cases the reconstruction errors are larger than those of the corresponding charm1 reconstructions. Our DESY5 reconstruction exhibits a noticeable upwards deviation from the flat ΛCDM comparison fields. Analysis of synthetic data indicates that if distance moduli at redshifts $z < 0.82$ were systematically increased, our algorithm could produce such a feature. Previous studies, however, report systematic offsets in DESY5 distance moduli only at $z < 0.1$. If the DESY5 data are not affected by unaccounted systematics, the observed deviation could be indicative of evolving dark energy.

Key words. Cosmic Energy Density – Non-Parametric Bayesian Inference – Information Field Theory – Supernovae Ia

1. Introduction

The detection of the universe's accelerated expansion by Perlmutter et al. (1999) implied that most of the universe's energy content is due to an unknown energy density contribution, dubbed the "dark energy" ρ_Λ, which appears to remain constant even as the universe expands. Together with observations providing strong evidence for the existence of a cold dark matter component (weak lensing map of the bullet cluster, rotation curves of galaxies etc; see Freese (2009) for a review), the so-called ΛCDM model has been the favored candidate for a standard model of cosmology. Peculiarly, cosmological analyses based on this model revealed that only about 5% of all matter in the universe is made up of "ordinary" baryonic matter, with approximately 95% bound up in the dark matter and dark energy component (Freese 2009).

Thus, astronomy finds itself in a situation where only a fraction of the universe's energy content is understood, and possible tensions between theoretical predictions and observations are examined to gain insight into the nature of these unknown components.

In recent years, models that allow the dark energy density ρ_Λ to evolve over cosmic time have regained traction, with new analyses favoring such a dynamical dark energy scenario (Adame et al. 2025). Often, studies lay out a parametric form for the evolution of the dark energy component. Cosmological parameters, such as the relative energy density fractions in the universe, can then be extracted by minimizing the χ^2 between the predicted and observed data with respect to the parameters of interest. This methodology assumes that the model used (e.g. the ΛCDM model or the parametric evolution of the dark energy component) is valid in the first place. If it is not, this introduces bias into the result.

To circumvent such model bias, different methods have been developed to viably extract cosmological insights from observed data without assuming a specific physical model, and or without laying out a specific parametric form for the to be inferred quantity. In the case of the former, we speak of an "agnostic inference", and in the case of the latter, of a "non-parametric inference". Some popular non-parametric reconstruction methods are Gaussian Processes (Holsclaw et al. 2010, 2011; Shafieloo et al. 2012; Seikel et al. 2012; Jiang et al. 2024; Mukherjee & Sen 2024), Principal Component Analyses (PCA) (Ishida & de Souza

2010; Sharma et al. 2022), Splines and other polynomial-based approaches (for example Padé-Polynomials) (Joy et al. 2019; Benetti & Capozziello 2019; Jiang et al. 2024), as well as smoothing approaches (Shafieloo et al. 2006; Matthewson & Shafieloo 2024). In recent years, Neural-Network-based reconstructions have emerged as well (Mukherjee et al. 2022; Zhang et al. 2024).

Porqueres et al. (2017) proposed a non-parametric and agnostic approach to reconstruct the evolution of the cosmic expansion in the late universe through Supernovae Ia (SNIa) inside the framework of information field theory (IFT) (Enßlin et al. 2009). In that work, the so-called "response operator" is linearized and the posterior distribution found with a Wiener filter. This solution is perturbed and the Wiener filter applied again, until the solution is stationary. This essentially describes an iterative maximum-a-posteriori scheme, where the mode of the posterior is approximated by a Gaussian.

Here we extend this approach by using the geometric variational inference (`geoVI`, Frank et al. 2021) algorithm to account for the non-linear terms of the data model and provide more accurate uncertainties of the posterior results.

Rather than defining constant piecewise functions (Zheng & Li 2017) for the equation of state parameter or polynomials (Sharma et al. 2022) for the Hubble parameter, our method does not rely on a functional basis, accounting for all the eigenmodes of the Fisher information metric as opposed to a principal component analysis. Our approach refines hyperparameters, a feature it shares with some neural-network frameworks (e.g., Zhang et al. (2024)), while not requiring the training on datasets.

In this paper, we present `charm2` (cosmic history agnostic reconstruction method No. 2), a code for non-parametrically reconstructing the redshift evolution of the universe's energy density, with improved treatment of the inference problem's non-linearities, when compared to its predecessor in Porqueres et al. (2017). `charm2` is built using the Python package `NIFTy` (v8[1]).

The paper is structured as follows: In Sect. 2, we revisit standard cosmological ideas and explain how these ideas serve as a guide to design an agnostic inference approach of the cosmic expansion history. The to-be-inferred signal and the data model are defined, before the data sets analyzed in this work are described in Sect. 3. Finally, we present our results in Sect. 4 and summarize our findings in Sect. 5.

2. Inference approach

2.1. Basic theory and signal definition

Conceptually, the standard ΛCDM model of cosmology rests upon the cosmological principle, the notion that matter is distributed homogeneously and isotropically on the largest scales of space. On these scales, matter is described as a type of fluid, the "perfect fluid", which is often modeled through the particularly simple equation of state (EOS)

$$p_i = w_i \rho_i, \tag{1}$$

where ρ_i, p_i and w_i are the fluids energy density, pressure, and so-called EOS parameter, respectively. In the ΛCDM model, the EOS parameter w is assumed to be a constant for each fluid i contributing to the universe's total energy density ρ:

$$\rho = \sum_i \rho_i = \sum_i \rho_{0i} a^{-3(1+w_i)}. \tag{2}$$

[1] `NIFTy` (numerical information field theory) is available at https://ift.pages.mpcdf.de/nifty/user/index.html

Here, ρ_{0i} represents the energy density value of the i-th contribution today and a is the scale factor. Contributions may include ordinary and dark matter (collectively called "dust"), radiation, the dark energy and the universe's intrinsic curvature, denoted by ρ_m, ρ_r, ρ_Λ and ρ_k respectively.

One may then solve the Einstein field equations to determine the universe's evolution through its expansion rate, quantified by the Hubble parameter,

$$H(a) = \frac{\dot{a}}{a}. \tag{3}$$

The expansion rate is related to the universe's total energy density via the first Friedmann equation:

$$H(a)^2 = \frac{8\pi G}{3}\rho \overset{\text{Eq. (2)}}{=} \frac{8\pi G}{3}\left(\rho_{0m}a^{-3} + \rho_{0r}a^{-4} + \rho_{0k}a^{-2} + \rho_{0\Lambda}\right). \tag{4}$$

Here, the dependence on the scale factor a is characteristic for each type of fluid, arising from different values of the EOS parameter w (e.g., $w = 0$ for dust, $w = 1/3$ for radiation and $w = -1$ for a constant dark energy).

Note how the evolution of each fluid in Eq. (4) is governed by a unique power law exponent. For example, towards the early universe when $a \ll 1$, the contribution due to radiation ($\propto a^{-4}$) becomes very large, dominating the total energy budget, while for $a \gg 1$, it will become more and more negligible. Therefore, at a given redshift, there is usually one dominating contribution to the total energy budget of the universe, subdividing the universe's life into different "eras".

In this work, we make no assumptions on the individual components contributing to the total energy density ρ and their evolution through cosmic time, since these are a priori not known. Since the universe may be expanding by multiple orders of magnitude, it is natural to define and investigate a "signal" s as the energy density on a double-logarithmic scale

$$s(x) := \ln\left(\frac{\rho(x)}{\rho_0}\right), \tag{5}$$

where $x = -\ln(a) = \ln(1+z)$ and ρ_0 is an arbitrary reference energy density.

As an example, the ΛCDM signal field $s_{\Lambda\text{CDM}}(x)$ takes on the form of a piecewise linear function in these coordinates: in the radiation dominated era, $\rho \approx \rho_{0r}a^{-4}$ and therefore $s_{\Lambda\text{CDM}}(x)$ is proportional to $-4 \cdot \ln(a)$ which in the x-coordinate just becomes a line of slope 4. Similarly, we have $\rho \approx \rho_{0m}a^{-3}$ for the matter dominated era and thus $s_{\Lambda\text{CDM}}(x) \propto 3x$, etc. One era is thus a linear function with slope proportional to its EOS parameter, connecting smoothly to the linear function representing the next era.

Here, we model $s(x)$ as a non-parametric, stationary process around a mean linear trend (see Sect. 2.4), by imposing homogeneous statistics on $s(x)$, i.e. letting its covariance S at two points x and y only depend on their difference:

$$S_{xy} = C_s(x - y),$$

with the 2-point-correlation function C_s. This description is justified by the following consideration:

By adding a non-parametric component to the linear evolution, the stationary component only needs to capture oscillations around a mean linear trend, where the amplitude of the oscillations only varies in one order of magnitude thanks to the log-log parameterization in Eq. (5). A stationary process is then well suited, since the variance $S_{xx} = C_s(0)$ is constant for all x and does not vary by orders of magnitude across the domain.

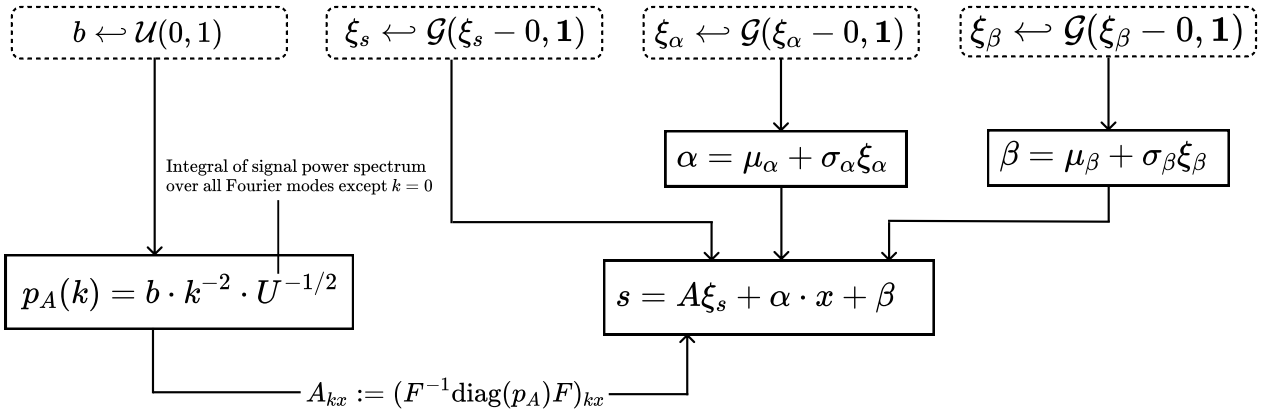

Fig. 1: The generative model used for the inference of the cosmic expansion history as encoded in $\ln(\rho/\rho_0)$ in charm2. The right side of the graph describes the generation of the linear part of charm2's model. The linearly evolving part of the signal s, $\alpha x + \beta$, should capture the dominant part of the density evolution and is that of a single cosmic constituent. On the left side of the graph, the generation of the non-parametric $A\xi_s$ part of the signal is shown. The non-parametric part allows the model to flexibly deviate from a single component equation of state. The random variates α, β, n and b are described by the distributions shown in Table 1.

Finally, the aforementioned parametric form of the ΛCDM signal field can be used to motivate the functional form of the power spectrum describing the statistical process (see Sect. 2.3).

2.2. Instrument response

To constrain the expansion history of the universe, one measures the redshifts of objects at cosmological distances. The way redshift varies with distance encodes information about how the universe has expanded over time.

In particular, when inferring distances from the observed flux emitted by distant objects, the appropriate distance measure is the luminosity distance, which in a flat universe and assuming the FLRW metric takes the form

$$d_L(z) = (1+z)\int_0^z \frac{c}{H(\tilde{z})}\,\mathrm{d}\tilde{z}. \tag{6}$$

Through a multi-step calibration process known as the cosmic distance ladder, this distance measure can be connected to the observed distance modulus of type Ia supernovae via

$$\mu = 5\log_{10}(d_L^{(\mathrm{pc})}) - 5, \tag{7}$$

where $d_L^{(\mathrm{pc})}$ denotes the luminosity distance in units of pc. These distance moduli constitute our discrete set of data d, which depend on the physical quantity $s = \log(\rho/\rho_0)$ we want to infer in the following way: the energy density determines the evolution of the Hubble parameter through the first Friedmann equation. The Hubble parameter in turn influences the luminosity distance via Eq. (6).

Through our signal definition Eq. 5, the Hubble parameter can be expressed as

$$H^2(x) = \frac{8\pi G}{3}\rho(x) = \frac{8\pi G}{3}\rho_0 e^{s(x)}. \tag{8}$$

Note that here, the reference energy density ρ_0 is chosen as

$$\rho_0 = 10^6 \frac{\mathrm{kg}}{\mathrm{m}\cdot\mathrm{Mpc}^2}, \tag{9}$$

such that the Hubble-Parameter is in the usual units of km/s/Mpc: $[H(a)] = \sqrt{[G]\cdot[\rho]} = \sqrt{[G]\cdot\rho_0} = \mathrm{km/s/Mpc}$, where G is Newton's gravitational constant in SI-units.

In the language of IFT, the function that maps the signal to the (noiseless) data is defined as the response operator. This function encapsulates the complex physical processes leading to the data generation. Using the SN Ia distance modulus, Eq. (7), together with Eq. (8) allows us to write the response operator as

$$R_x(s) = 5\log_{10}\left(e^x \mathcal{K}\int_0^x e^{-\frac{1}{2}s(\tilde{x})+\tilde{x}}\,\mathrm{d}\tilde{x}\right) - 5, \tag{10}$$

where $\mathcal{K}$ is a constant defined as

$$\mathcal{K} = 1000\cdot c\left(\frac{8\pi G}{3}\right)^{-\frac{1}{2}}, \tag{11}$$

with c and G implicitly given in SI-units. The constant $\mathcal{K}$ is chosen such that the requirement of the luminosity distance, as expressed in Eq. (7), to be in pc, is met: the line-of-sight integral is implicitly an integral over $c/H(x)$ which is in $1000\cdot$ pc since $H(x)$ is in km/s/Mpc. Expressing $H(x)$ in terms of the signal field $s(x)$ through Eq. (8) introduces the additional $8\pi G/3$ factor. Where appropriate, we will write $\hat{H}_0$ to indicate a Hubble constant implicitly given in km/s/Mpc, instead of writing out the unit explicitly.

Assuming additive noise, n, the data can be written as

$$d = R(s) + n =: s' + n, \tag{12}$$

where s' is referred to as the noiseless data.

Finally, given the posterior mean of the signal, s^*, a posterior H_0 value can be obtained non-parametrically through

$$H_0 = H(x=0) = \left(\frac{8\pi G}{3}\rho_0 e^{s_0^*}\right)^{1/2}, \tag{13}$$

with the inferred $s_0^* := s^*(x=0)$. However, as we discuss in Sect. 3, distance moduli of SN Ia require a fiducial H_0 value for their calibration.

2.3. Inference method

Our inference method recovers the posterior distribution of the signal given the data, $\mathcal{P}(s\,|\,d)$, which is given by the Bayes' Theorem as

$$\mathcal{P}(s\,|\,d) = \frac{\mathcal{P}(d\,|\,s)\mathcal{P}(s)}{\mathcal{P}(d)}, \tag{14}$$

where $\mathcal{P}(d\,|\,s)$ is the likelihood, $\mathcal{P}(s)$ is the signal prior and the normalisation $\mathcal{P}(d)$ is the evidence. In IFT, the evidence is redefined as a partition function,

$$\mathcal{Z}(d) := \mathcal{P}(d) \tag{15}$$

and negative log-probabilities as information Hamiltonians,

$$\mathcal{H} = -\ln(\mathcal{P}). \tag{16}$$

Then, Bayes' Theorem is given by

$$\mathcal{P}(s\,|\,d) = \frac{1}{\mathcal{Z}} e^{-\mathcal{H}(s,d)} = \frac{1}{\mathcal{Z}} e^{-\mathcal{H}(d\,|\,s)-\mathcal{H}(s)}. \tag{17}$$

In order to apply Bayes' Theorem, a likelihood term $\mathcal{H}(d\,|\,s)$ and prior $\mathcal{H}(s)$ have to be chosen. We are provided with the uncertainty variance of the magnitude data. Given no further information on the data statistics, a Gaussian likelihood function is the natural assumption then, according to the Maximum Entropy principle. Therefore, $\mathcal{H}(d\,|\,s)$ is chosen as the following quadratic form:

$$\mathcal{H}(d\,|\,s) \mathrel{\widehat{=}} \frac{1}{2}(d - R(s))^\dagger N^{-1}(d - R(s)), \tag{18}$$

where $\mathrel{\widehat{=}}$ denotes equality up to constants.

A priori, we assume that the matter distribution in the universe is homogeneous and isotropic on large scales and that the total energy density ρ evolves smoothly with the scale factor, while it potentially may vary over multiple orders of magnitude. As discussed in Sect. 2.1, defining the signal s as $s(x) = \ln(\rho(x)/\rho_0)$ where $x = -\ln(a)$, the amplitude of these variations becomes comparable among the different eras of the universe (matter domination, radiation domination, etc.). A stationary, also known as a homogeneous process, is then well suited, since its covariance is given by

$$S_{xy} = C_s(x - y), \tag{19}$$

where C_s is again the signal's 2-point-correlation function. This leads to the variance being constant over the whole x-domain, $S_{xx} = C_s(0)$, reflecting that s exhibits fluctuations of comparable amplitude across all eras in the x-coordinate.

Thus, the prior term $\mathcal{H}(s)$ too is chosen as a quadratic form with a stationary covariance matrix as in Eq. (19). Instead of storing a dense matrix, note that the Wiener-Khinchin theorem states that such a covariance matrix becomes diagonal in Fourier space*:

$$\tilde{S}_{kq} = 2\pi \cdot \delta(k - q) p_s(k), \tag{20}$$

where the diagonal elements are given by the signal power spectrum $p_s(k)$.

Following the argumentation of Porqueres et al. (2017), the a priori signal power spectrum $p_s(k)$ is given by

$$p_s(k) = vk^{-4}, \tag{21}$$

where v determines the amplitude of field fluctuations. The exponent of -4 stems from the following consideration.

As outlined already in Sect. 2.1, by defining the signal domain as $x = -\ln(a) = \ln(1+z)$, the ΛCDM signal $s_{\Lambda\mathrm{CDM}}(x)$ takes on the form of a piecewise-linear function. Each line segment's slope is proportional to the EOS parameter of the fluid with dominant contribution to the total energy density at the given redshift.

Therefore, curvature in the signal field is only expected at redshifts at which a transition between regimes occurs, meaning highly curved signal fields are improbable.

A measure for the total curvature of a field is given by taking the field's Laplacian, absolute squaring it for positiveness and integrating: $C := \int \mathrm{d}x\, |\Delta s(x)|^2$. Taking the scalar product to be the L^2-norm, this may be rewritten as $C = s^\dagger(\Delta^\dagger\Delta)s$. Identifying $S^{-1} := v^{-1}\Delta^\dagger\Delta$ and Fourier-transforming leads to the exponent -4 in Eq. (21).

Thus, S^{-1} takes on the function of a smoothing kernel and the constant v is a scaling constant that determines how much the probability of highly curved signal realizations is weighed down in the inference. This constant was set to $v = 1$ in Eq. (21) by Porqueres et al. (2017). Here, however, while we assume the same power law dependence of Eq. (21), we adapt the strength of the smoothing constant v to what the data demands by making it part of the inference. More specifically, we replace the fixed parameter v with a related quantity, the fluctuation parameter b, which captures fluctuations around a mean trend (see Sect. 2.4 for motivation). In Porqueres et al. (2017), the field variance at each point scales with v, as given by $\langle s^x s^{x^*}\rangle_{(s)} = v\int_{k>0} k^{-4}\mathrm{d}k$. In contrast, our model directly sets the variance as $\langle s^x s^{x^*}\rangle_{(s)} = b^2$.

When the data, prior and likelihood terms are defined, one only needs to apply Bayes' Theorem, Eq. (17), to infer the posterior distribution of the signal. However, analytical solutions are often not possible and, in many cases, the partition function $\mathcal{Z}$ makes the problem intractable analytically or too computationally expensive (Knollmüller & Enßlin 2018).

Variational inference (VI) addresses this problem. The posterior $\mathcal{P}(s\,|\,d)$ is not found directly, but rather approximated through a trial distribution, leveraging the Kullback-Leibler divergence as a measure of dissimilarity between two probability distributions.

Knollmüller & Enßlin (2020) have proposed a Gaussian distribution for the trial distribution. The posterior however will often exhibit non-Gaussian features, leading to a sub-optimal approximation. In this work, we employ the `geoVI` algorithm (Frank et al. 2021), which finds a coordinate transformation that effectively absorbs potential curvature the posterior might exhibit. Thus, in this new coordinate system, the posterior is well approximated by a Gaussian distribution.

2.4. Generative model prior

As prior information, we assume that the universe evolves monotonically (expanding, contracting or static universe) in a smooth fashion. The monotonicity of the evolution is captured through a linear model:

$$s_{\mathrm{lin}} = \alpha x + \beta, \tag{22}$$

where α and β are variables, a prior assumed to be drawn from Gaussian distributions, representing the slope and offset of the linear evolution. Deviations about this linear evolution are modeled via the so-called Correlated Field Model (CFM). The CFM, introduced in Arras et al. (2021) and Arras et al. (2022) creates field realizations using a power spectrum based on a parametric form with contributions from stochastic processes:

$$s_{\mathrm{CFM}} = A\xi_s, \tag{23}$$

where A is the so-called amplitude operator and ξ_s is a Gaussian standard variable, $\xi_s \hookleftarrow \mathcal{G}(0, \mathbf{1})$. In Fourier space, the diagonal

elements of the amplitude operator are given by the amplitude spectrum $p_A(k)$, which in turn is related to the signal power spectrum via $p_A(k) = \sqrt{p_s(k)}$ (see App. A).

In this work, we will assume a pure power-law form of the amplitude spectrum:

$$p_A(k) = b \cdot \frac{k^n}{\sqrt{U}}, \tag{24}$$

where $U = \int_{k\neq 0} \mathrm{d}k\, k^{2n}$ normalizes the amplitude spectrum such that the real-space variance of the field is exactly controlled by the fluctuations parameter b: $\langle s^x s^{x^*} \rangle = \int_{k\neq 0} \mathrm{d}k\, p_A(k)^2 = b^2$.

Adding the contribution by the linear model and the CFM gives us one signal realization:

$$s = s_{\mathrm{lin}} + s_{\mathrm{CFM}} = \alpha x + \beta + A\xi_s. \tag{25}$$

A flowchart of this forward model can be seen in Fig. 1.

Table 1 shows the names, distributions, and prior mean and standard deviation of the hyperparameters. Here we discuss these prior choices:

- α: the prior mean slope of the line model is set to 2. The standard deviation is set to the same order of magnitude as the prior mean to guarantee sufficient flexibility of the model.
- β: the prior mean is chosen as the $s(x = 0)$ value of flat ΛCDM cosmology fields (cf. Fig. 6), again with a standard deviation in the same order of magnitude
- n: is set to -2 according to Eq. (21). Notice that this is a factor of $1/2$ smaller than the exponent found in Eq. (21) to account for the fact that $p_s(k) = \sqrt{p_A(k)}$
- b: drawn from a uniform distribution $\mathcal{U}$ in the interval $[0, 1]$ to be maximally agnostic (see Fig. 2). The order of magnitude of this parameter is gotten by comparing to a reference value, $b_{\Lambda\mathrm{CDM}}$, the expected fluctuations in case of a flat ΛCDM cosmology. This reference value was obtained through a linear best-fit to a reference field constructed using the Planck2018 (Planck Collaboration 2020) cosmology parameters and found to be $b_{\Lambda\mathrm{CDM}} \approx 0.14$. Therefore, drawing b from $\mathcal{U}(0, 1)$ should allow for enough flexibility to construct any non-ΛCDM features should the data wish it.

Periodic boundary conditions are enforced by the correlated field model due to Fast-Fourier-Transforms involving the power spectrum. To avoid artifacts due to periodic boundary conditions, we extend the signal domain by a factor of 2 and introduce a zero-padding mask in the margins to reduce its impact on the likelihood (Arras et al. 2021).

Table 1: Hyperparameters chosen for the generative prior model. Gaussian and uniform distributions are denoted by $\mathcal{G}(\mu', \sigma')$ and $\mathcal{U}(l', u')$, where μ', σ', l' and u' are the mean, standard deviation, lower and upper bound respectively.

Description	Symbol	Distribution
Slope of line model	α	$\mathcal{G}(2, 5)$
Offset of line model	β	$\mathcal{G}(30, 10)$
Power law exponent of amplitude spectrum	n	$\mathcal{G}(-2, 10^{-16})$
Fluctuations	b	$\mathcal{U}(0, 1)$

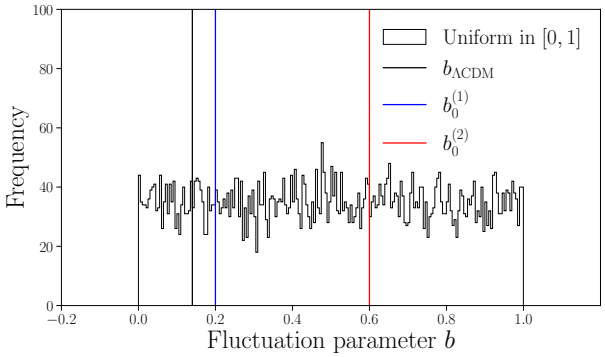

Fig. 2: Prior samples for the free model parameter "fluctuations", b, which are drawn from a uniform distribution in the interval $[0, 1]$. This parameter sets the a priori expected level of field fluctuations around the field mean. We use the fluctuations parameter expected from a flat ΛCDM model, $b_{\Lambda\mathrm{CDM}}$ (black vertical line), to set an appropriate scale for this distribution heuristically (see App. B). The blue and red vertical lines indicate two possible starting positions for the inference scheme, which were used in the real data reconstructions of this work.

3. Data

We use our inference method to analyze three SN Ia data sets: Union2.1 (Suzuki et al. 2012), Pantheon+ (Scolnic et al. 2022) and DESY5 (Dark Energy Survey Year 5) (DES Collaboration 2024).

The datasets consist of distance moduli μ obtained by fitting the SN light curves with spectral energy distribution templates (Kenworthy et al. 2021),

$$\mu = m + \chi x_1 - \psi y - M - \delta_{\mu-\mathrm{bias}}, \tag{26}$$

where $m = -2.5\log_{10}(x_0)$ is the apparent magnitude and M is the absolute magnitude; x_0, x_1 and y parametrize the lightcurve; and χ, ψ and $\delta_{\mu-\mathrm{bias}}$ are calibration parameters.

The absolute magnitude M is degenerate with H_0 regarding their effect on the SN Ia distance modulus. Many analyses therefore combine these two into one parameter (e.g., Perlmutter et al. (1999), Rubin et al. (2023) and DES Collaboration (2024)),

$$\mathcal{M} = M + 5\log_{10}(c/H_0), \tag{27}$$

which is jointly inferred with the cosmological parameters. Therefore, the distance moduli can only be obtained by assuming a value of H_0.

Union2.1 and DESY5 assume a value of $h := H_0/(100\mathrm{km/s/Mpc}) = 0.7$, while Pantheon+ uses Cepheids as a primary distance anchor to infer a value of H_0 from low-redshift measurements, allowing to lift the degeneracy in Eq. 27.

Figure 3 shows the redshift distributions of the datasets. The redshift ranges of the datasets are indicated in Table 2.

Table 2: Redshift range and number of datapoints of the data sets analysed in this work.

Dataset	$(\mathbf{z}_{\mathrm{min}}, \mathbf{z}_{\mathrm{max}}, \bar{\mathbf{z}})$	# Datapoints
Union2.1	(0.015, 1.414, 0.36)	580
Pantheon+	(0.00122, 2.26, 0.22)	1701
DESY5	(0.025, 1.12, 0.46)	1829

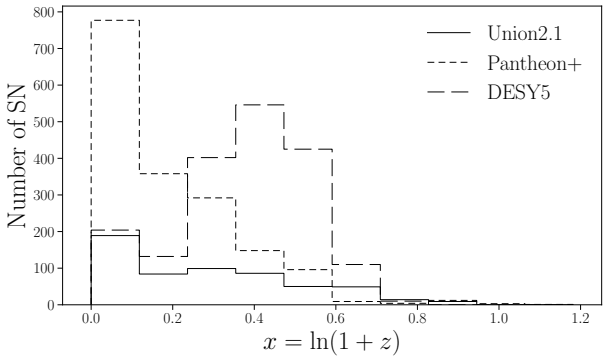

Fig. 3: Histograms of the used data sets binned in ten x bins. While the Pantheon+ sample dominates the low redshift regime, the new DESY5 sample shows a significant boost in the number of mid-to-high redshift SN samples.

4. Results

4.1. Impact of b initialization on field reconstruction

In this section, we apply the `charm2` algorithm to synthetic and real data, to both validate our inference method and reconstruct the posterior mean field of $s = \ln(\rho/\rho_0)$ for our universe.

To speed up computation, the inference can be initialized with a field that's a reasonable first guess. If the priors are broad enough and the probability landscape has no significant local minima, this introduces minimal bias, as it simply allows the algorithm to converge faster than when starting from a field we deem to be far from the posterior field under our prior knowledge.

For example, the initial fluctuation parameter, b_0, may be set to lie close to the value expected from ΛCDM, e.g., $b_0^{(1)} = 0.2$ (compare against $b_{\Lambda\mathrm{CDM}} \approx 0.14$), or may be set to a value triple that, $b_0^{(2)} = 0.6$ (see vertical colored lines in Fig. 2).

Since the data values are line of sight integrals over $x = -\ln(a)$, signal fields that oscillate at a high rate around their mean line (e.g., in case of $b_0^{(2)} = 0.6$) give approximately the same data as signal fields that show much more damped oscillations (e.g., in case of $b_0^{(1)} = 0.2$). Therefore, the field fluctuations of $s = \ln(\rho/\rho_0)$ cannot be constrained from SN alone.

We thus present our results in terms of the fluctuation parameter b, showcasing reconstructions where this parameter was initialized at lower values, $b = b_0^{(1)} = 0.2$ and higher values $b = b_0^{(2)} = 0.6$. Where appropriate, we discuss reconstructions at the very low fluctuations scale, e.g. $b \sim 0.05$.

4.2. Synthetic reconstruction

We validate the inference method with synthetic datasets generated via a flat ΛCDM model corresponding to $\Omega_{\mathrm{m0}} = 0.3$. Each dataset contains 500 datapoints, but the distribution over redshift varies as:

1. Dataset 1: the redshifts are sampled from a normalized uniform distribution within the redshift range, $\mathcal{P}(z) = \mathrm{cst}$.
2. Dataset 2: the density of data points decays with redshift exponentially. The redshifts are sampled from the normalized distribution $\mathcal{P}(z) = \frac{1}{2}e^{-\frac{1}{2}z}$ and then rescaled to lie within the desired redshift range.

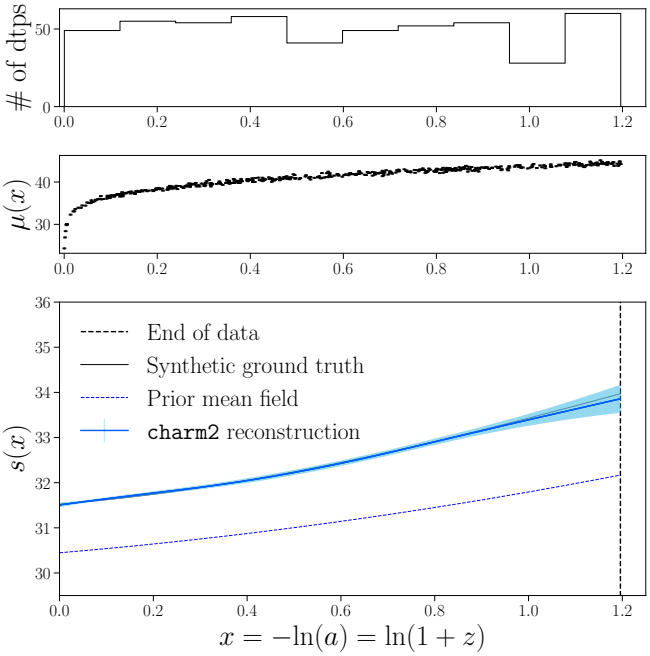

Fig. 4: Reconstruction of a synthetic data set in `charm2`. From top to bottom: Histogram of the number of data points; the data plotted as a function of the x-coordinate; and the prior mean field (dashed blue line) along with the posterior mean field (solid blue line) with its 1σ uncertainty band (shaded blue region), and the ground truth (solid black line). The inference was initialized with a fluctuation parameter of $b_0 = 0.2$. The assumed noise variance on the synthetic data of $\sigma_n^2 = 0.1$ makes the errorbars vanishingly small compared to the scale of the y-axis.

The redshifts and signal fields are then mapped into the data space through the response operator, Eq. (10), after which Gaussian and independent noise samples are added to mimic the dispersion of the data points.

The noise variance was set to 0.1, motivated by the mean variance of data points in the Union2.1 compilation (≈ 0.07).

For an initial fluctuation parameter of $b_0 = 0.2$, as shown in Fig. 4 (Dataset 1) and 5a (Dataset 2), our inference method recovers the true signal across the redshift range for both synthetic datasets. For Dataset 2 (Fig. 5a), the reconstruction uncertainty increases at high x, where fewer data points are available.

By comparing Fig. 5a ($b_0 = 0.2$) and 5b ($b_0 = 0.6$), we can assess that the analysis of synthetic data is robust against different initializations of the fluctuation parameter: The posterior mean fields agree within their reconstruction error.

4.3. Union2.1, Pantheon+ and DESY5 reconstructions

We applied `charm2` to the Union2.1, Pantheon+ and DESY5 datasets. We compare our reconstructions to flat ΛCDM reference fields shown in Fig. 6, s_{CMB} and s_{SN}, corresponding to the signal for the cosmological parameters found by the Planck2018 (Planck Collaboration 2020) and the Pantheon+SH0ES (Brout et al. 2022) analyses, respectively (see App. B for construction).

The reconstructed fields for the three datasets are presented in Fig. 7, alongside histograms of their respective redshift distributions.

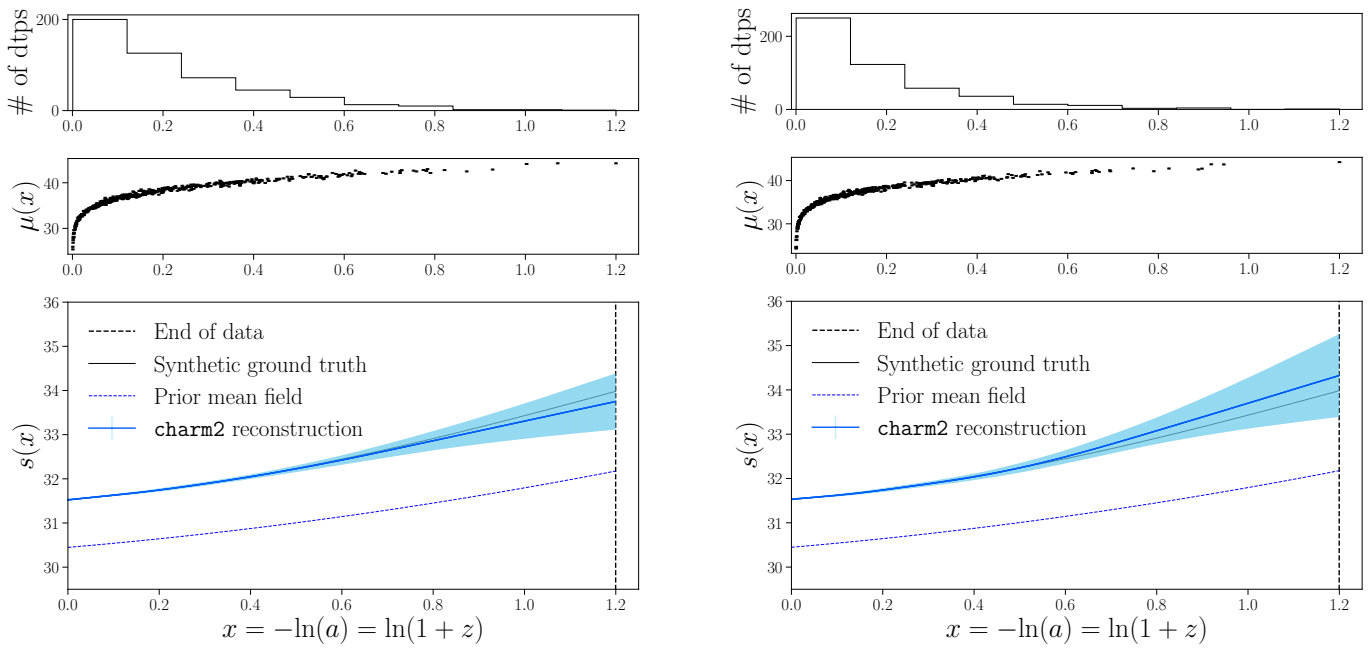

(a) Initial fluctuations parameter $b_0 = 0.2$.

(b) Initial fluctuations parameter $b_0 = 0.6$.

Fig. 5: Reconstruction of synthetic datasets with an exponential decrease in the number of datapoints with redshift in charm2. The bottom panel shows the prior mean field (dashed blue line) along with the posterior mean field (solid blue line) with its 1σ uncertainty band (shaded in blue), and the ground truth (solid black line). The subcaptions indicate the fluctuation parameter at which the inference was initialized. Note that the difference in the prior mean field is an effect of these different initializations. As in Fig. 4, the variance on the data $\sigma_n^2 = 0.1$ is small compared to the scale of the y-axis, making the errorbars invisible.

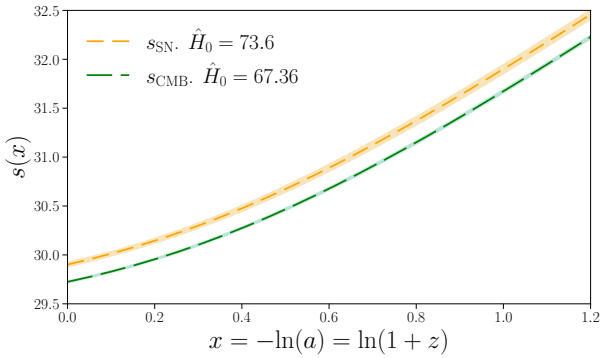

Fig. 6: Mean field and estimated 1σ region for the flat ΛCDM models with the Ω_m and H_0 values from Planck2018 (green) and Pantheon+SH0ES (orange). The 1σ contour was estimated through Gaussian error propagation of the uncertainties of the values in Table B.1 into Eq. (B.2), which assumes H_0 and Ω_m are independent. These fields serve as benchmarks for our reconstructions.

Union2.1

In the case of Union2.1, we compare our results to the previous charm1 analysis of the same data. While the reconstructed fields are compatible, charm2 provides more realistic uncertainties by better accounting for the nonlinearities of the response operator, which were neglected in Porqueres et al. (2017). This demonstrates the advantage of non-Gaussian posterior approximation techniques. We also show the effect of changing charm2's initial fluctuations parameter from $b_0 = 0.2$ to $b_0 = 0.6$. The results are compatible, showing that the analysis is robust to the choice of b_0, which only affects the uncertainty at high-redshifts where the data is less constraining.

Note that the here-in used Union2.1 data used a fiducial value of $H_0 = 70$km/s/Mpc to report the distance modulus μ (see data section, Sect. 3). This fixed H_0 value biases the reconstruction towards lower energy densities at $z = 0$, making it lie closer to the $s_{\rm CMB}$ field.

Pantheon+

The analysis of the Pantheon+ data shows equivalent results: the analysis is robust to the choices of b_0, providing reconstructed fields that are compatible within the $1-\sigma$ uncertainty.

We note that the Pantheon+ reconstruction is compatible with $s_{\rm SN}$ and incompatible with $s_{\rm CMB}$. This is likely a manifestation of the Hubble Tension, as already noted in one of the Pantheon+ analysis papers (Riess et al. 2022): Measurements of the acceleration rate using the cosmic distance ladder differ from extrapolations based on cosmological analyses of the CMB.

DESY5

When setting the b_0 parameter to 0.6 or 0.2, the analysis of DESY5 data shows a change of behaviour at $x \sim 0.45 - 0.75$ (corresponding to redshift $z \sim 0.57 - 1.17$). At this redshift range, the reconstructed fields deviate from the parametric flat ΛCDM reference fields. Given the recent results from the DES Collaboration (2024), we compare our DESY5 reconstruction to an evolving dark energy signal, where the equation of state of dark energy follows

$$w_\Lambda(a) = w_0 + w_a(1-a), \tag{28}$$

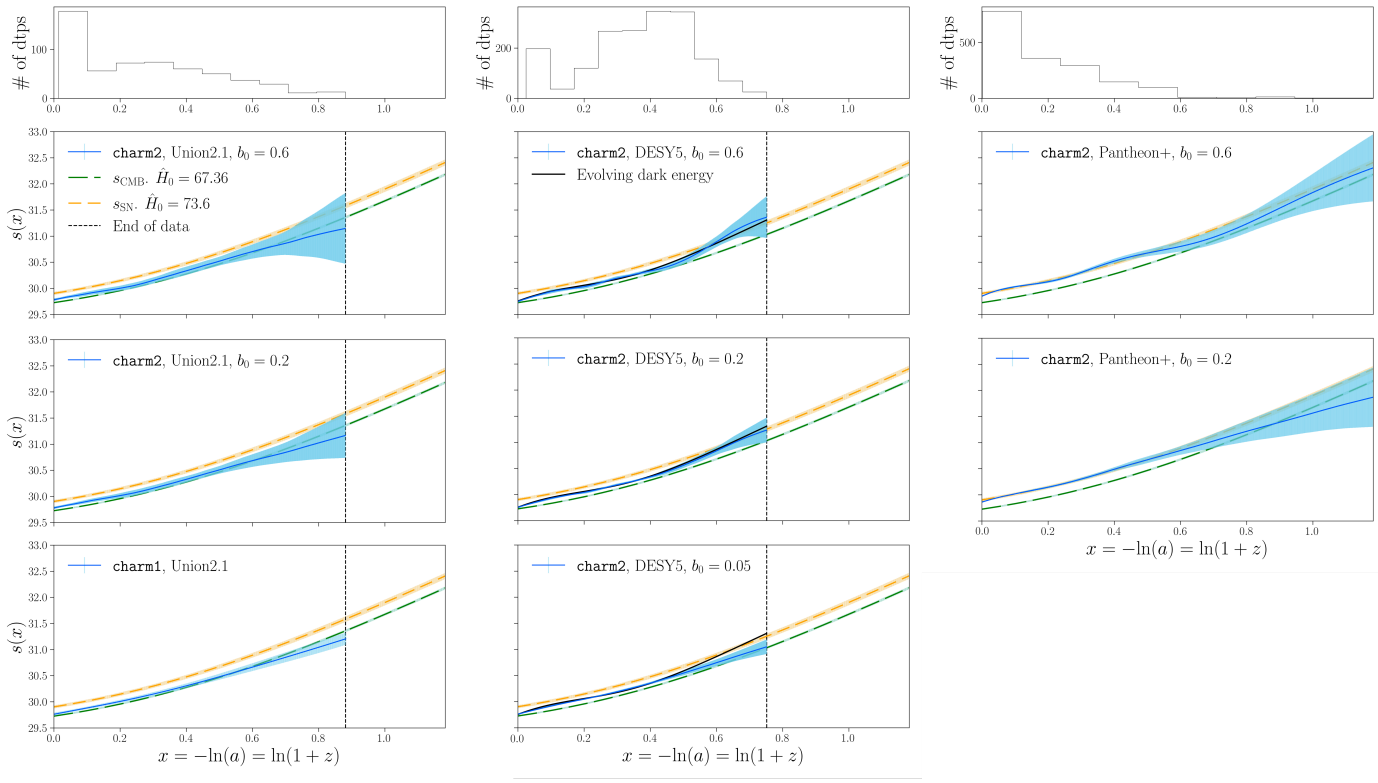

Fig. 7: charm2 reconstructions for Union2.1 (left column), DESY5 (middle column) and Pantheon+ (right column) and different fluctuation parameter initial values b_0 (rows). In each panel the posterior mean-field (solid blue line) and its 1σ confidence region (shaded blue region) are displayed alongside the reference fields of Fig. 6 (dashed orange and green lines). Additionally, for the DESY5 reconstruction, the signal field corresponding to the evolving dark energy model suggested by DES Collaboration (2024) ($(\Omega_m, w_0, w_a) = (0.495, -0.36, -8.8)$) is shown as the black solid line. Since H_0 is not constrained in the latter analysis, we choose a H_0 value of 68km/s/Mpc, manually fixing the y-offset of the evolving dark energy field to a value near the y-intersection of our own reconstruction. A comparison with the previous charm1 analysis of Union2.1 is shown in the left column (lower panel), where the signal definition is adapted as described in App. C.

with the parameter values found by the DES Collaboration (2024),

$$(\Omega_m, w_0, w_a) \approx (0.495, -0.36, -8.8). \tag{29}$$

Our DESY5 reconstruction is compatible with the varying dark energy signal for values of $b_0 = 0.6$ and $b_0 = 0.2$, assuming an approximate Hubble constant of $H_0 = 68$km/s/Mpc.

However, for values of $b_0 \lesssim 0.1$, this feature flattens out and deviates from the varying dark energy signal. We note that such a b_0 value significantly increases the stiffness of the model.

Since Efstathiou (2025) indicated a systematic offset of around 0.04 mag between the low-and high-redshift data of the Pantheon+ and DESY5 compilations, we investigated whether an offset of this magnitude can impact our reconstructed fields. Figure 8 shows a reconstruction from synthetic data based on a flat ΛCDM model, where all data points with $x < 0.6$ have been uniformly shifted by +0.1 mag. The reconstructed field shows a deviation similar to our DESY5 analysis, indicating that a systematic shift of this order can explain the feature in our DESY5 reconstruction. However, we could not identify a systematic offset in the low redshift regime $x < 0.1$ that reproduces such a feature, which is the regime where Efstathiou (2025) found $\langle m_{\rm Pantheon+} - m_{\rm DESY5} \rangle = (-0.051 \pm 0.007)$ mag. Furthermore, Vincenzi et al. (2025) indicated that this discrepancy between DESY5 and Pantheon+ arises from improvements of their analysis pipeline, leaving a potential systematic offset of the order of only 0.008 mag, which does not have a significant impact in our reconstruction results.

While systematic shifts at low x in our synthetic data analysis failed to reproduce the deviations observed in the DESY5 reconstruction, other systematic effects in the DESY5 data might still account for the non-flat-ΛCDM behaviour in the reconstruction due to the nonlinear effect of the noise covariance.

5. Conclusions

We have presented charm2, a Bayesian method to reconstruct the cosmic expansion from supernova data using information field theory. charm2 improves over charm1 (Porqueres et al. 2017) by providing more accurate uncertainties and accounting for the non-linearity of the data model, which is achieved by using the geometric variational inference algorithm (Frank et al. 2021). charm2 also uses a flexible Bayesian hierarchical model that permits inference of central quantities, such as the mean background cosmology and the statistical power spectrum, jointly to the quantities of interest. This ensures that charm2 is insensitive to biases arising by assuming a cosmological model.

We demonstrated that the analyses produce well-constrained posterior distributions even when the priors of the Gaussian variables of the model are set very broadly.

We tested the effect of choosing various initial fluctuation parameters b_0, which regulate the expected deviations from the

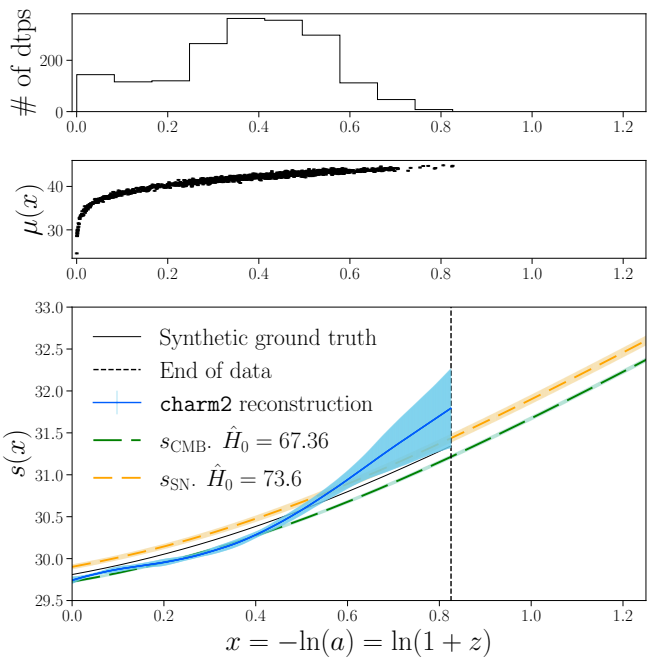

Fig. 8: Reconstruction from a synthetic dataset generated with a flat ΛCDM model with $\Omega_{\rm m0} = 0.3$ and $H_0 = 70.3$km/s/Mpc, where all data points $x < 0.6$ were systematically shifted by +0.1 mag. We adjusted H_0 so that the synthetic reconstruction resembles the DESY5 reconstruction, in order to evaluate whether a systematic offset might account for the DESY5 results.

mean background cosmology. In case of synthetic data, as well as Union2.1 and Pantheon+ data, the resulting reconstructs are robust against the initial choice of b_0, leading to fields that are compatible with the flat ΛCDM parametric form.

At lower redshifts, the Pantheon+ reconstruction is compatible with the signal field generated by the cosmological parameters of the Pantheon+SH0ES (Brout et al. 2022) analysis. The fact that it is strictly incompatible with the corresponding signal field generated by the Planck2018 (Planck Collaboration 2020) parameters is likely a reflection of the existing Hubble Tension between this SN dataset and measurements of the CMB, which was already noticed by the authors of the Pantheon+ analysis (Riess et al. 2022).

Meanwhile, the Union2.1 reconstruction is mostly compatible with the signal field generated by the Planck2018 analysis. This is likely due to the used data inherently assuming a fixed value of H_0 biasing the reconstruction towards lower energy density values.

The reconstruction from the DESY5 dataset presents a significant deviation from the parametric flat ΛCDM model at $x \gtrsim 0.45$ ($z \gtrsim 0.57$) for initial fluctuation values of $b_0 \gtrsim 0.1$. We investigate whether a systematic increase of the distance moduli at $x < 0.6$, i.e. redshifts of $z < 0.82$ can explain this deviation. While Efstathiou (2025) indicated a systematic offset of supernovae between the DESY5 and Pantheon+ catalogues in the regime $z < 0.1$, we were not able to reproduce the DESY5 reconstruction feature in our synthetic reconstructions by modifying the data in that redshift range. While our DESY5 reconstruction is consistent with the evolving dark energy model with the parameters of the DES Collaboration (2024) analysis, a more detailed study of systematics in DESY5 data would be necessary to confirm this.

As future work, we leave the incorporation of the absolute magnitude M of SN Ia in our Bayesian Hierarchical Model, to be jointly inferred with the signal. This value for M can then be compared against the SN light curves to yield H_0-agnostic values for the distance moduli, which would permit the extraction of a non-theory-laden H_0 value from the charm2 analysis.

Summarising, we have developed a non-parametric and largely model-agnostic method to infer the cosmic history from SN data. This method improves the set of tools with which we can rationally question and investigate the impact of the assumptions on data.

Acknowledgements. The authors thank Hanieh Zandinejad for helpful discussions.

References

Adame, A., Aguilar, J., Ahlen, S., et al. 2025, Journal of Cosmology and Astroparticle Physics, 2025, 021
Arras, Bester, Perley, et al. 2021, A&A, 646, A84
Arras, P., Frank, P., Haim, P., et al. 2022, Nature Astronomy, 6, 259–269
Benetti, M. & Capozziello, S. 2019, Journal of Cosmology and Astroparticle Physics, 2019, 008
Brout, D., Scolnic, D., Popovic, B., et al. 2022, The Astrophysical Journal, 938, 110
DES Collaboration. 2024, ApJ, 973, L14
Efstathiou, G. 2025, Evolving Dark Energy or Supernovae Systematics?
Enßlin, T. A., Frommert, M., & Kitaura, F. S. 2009, Physical Review D, 80
Frank, P., Leike, R., & Enßlin, T. A. 2021, Entropy, 23, 853
Freese, K. 2009, EAS Publications Series, 36, 113–126
Holsclaw, T., Alam, U., Sansó, B., et al. 2010, Phys. Rev. Lett., 105, 241302
Holsclaw, T., Alam, U., Sansó, B., et al. 2011, Phys. Rev. D, 84, 083501
Ishida, E. & de Souza, R. 2010, Astronomy and Astrophysics
Jiang, J.-Q., Pedrotti, D., da Costa, S. S., & Vagnozzi, S. 2024, Non-parametric late-time expansion history reconstruction and implications for the Hubble tension in light of DESI
Joy, M., Knox, L., & Aylor, K. 2019, in American Astronomical Society Meeting Abstracts, Vol. 233, American Astronomical Society Meeting Abstracts #233, 356.02
Kenworthy, W. D., Jones, D. O., Dai, M., et al. 2021, The Astrophysical Journal, 923, 265
Knollmüller, J. & Enßlin, T. A. 2018, Encoding prior knowledge in the structure of the likelihood
Knollmüller, J. & Enßlin, T. A. 2020, Metric Gaussian Variational Inference
Matthewson, W. L. & Shafieloo, A. 2024, arXiv e-prints, arXiv:2409.02550
Mukherjee, P., Said, J. L., & Mifsud, J. 2022, Journal of Cosmology and Astroparticle Physics, 2022, 029
Mukherjee, P. & Sen, A. A. 2024, Model-independent cosmological inference post DESI DR1 BAO measurements
Perlmutter, S., Aldering, G., Goldhaber, G., et al. 1999, ApJ, 517, 565
Planck Collaboration. 2020, A&A, 641, A6
Porqueres, N., Enßlin, T. A., Greiner, M., et al. 2017, Astronomy & Astrophysics, 599, A92
Riess, A. G., Yuan, W., Macri, L. M., et al. 2022, The Astrophysical Journal Letters, 934, L7

Rubin, D., Aldering, G., Betoule, M., et al. 2023, Union Through UNITY: Cosmology with 2,000 SNe Using a Unified Bayesian Framework
Scolnic, D., Brout, D., Carr, A., et al. 2022, The Astrophysical Journal, 938, 113
Seikel, M., Clarkson, C., & Smith, M. 2012, JCAP, 06, 036
Shafieloo, A., Alam, U., Sahni, V., & Starobinsky, A. A. 2006, Monthly Notices of the Royal Astronomical Society, 366, 1081
Shafieloo, A., Kim, A. G., & Linder, E. V. 2012, Phys. Rev. D, 85, 123530
Sharma, R., Mukherjee, A., & Jassal, H. 2022, The European Physical Journal Plus, 137
Suzuki, N., Rubin, D., Lidman, C., et al. 2012, The Astrophysical Journal, 746, 85
Vincenzi, M., Kessler, R., Shah, P., et al. 2025, Comparing the DES-SN5YR and Pantheon+ SN cosmology analyses: Investigation based on "Evolving Dark Energy or Supernovae systematics?"
Zhang, J.-C., Hu, Y., Jiao, K., et al. 2024, The Astrophysical Journal Supplement Series, 270, 23
Zheng, W. & Li, H. 2017, Astroparticle Physics, 86, 1

Appendix A: geoVI transform and standardization

Any variable $s \hookleftarrow \mathcal{G}(s, S)$ can be reparameterized in terms of a standard normal "latent variable" $\xi_s \hookleftarrow \mathcal{G}(\xi_s, \mathbf{1})$. This shifts the complexity of the correlation structure within the probability distribution to the mapping between s and ξ_s, allowing to construct hierarchical prior models (see Fig. 1) more easily. For a Gaussian field s, the mapping is achieved by considering an amplitude operator $A = F^\dagger \sqrt{\widehat{p_s}}$, where F is a Fourier transform, and $\widehat{p_s}$ is an operator with the signal power spectrum (p_s) as its diagonal.

The field s can then be written as

$$s = A\xi_s, \tag{A.1}$$

which is a zero-mean, Gaussian variable with the covariance $\langle ss^\dagger\rangle_{(s)} = A\langle \xi_s\xi_s^\dagger\rangle_{(\xi_s)}A^\dagger = AA^\dagger = F^\dagger(\sqrt{\widehat{p_s}})^2F = S$. Note that the power spectrum p_s and by extension the amplitude operator A, is itself built from standard normal variables (cf. Fig. 1). All standard normal variables involved in generating the model are collected into a single vector ξ.

In order to then ensure that a Gaussian distribution, parameterized through a variable θ

$$Q_\theta(\xi) = \mathcal{G}(\theta, \Theta(\theta))$$

is a good approximating distribution in the optimization of the KL-divergence, geoVI performs a coordinate transformation that aims to flatten out potential curvature in the posterior distribution.

In order to extract geometrical information from the posterior distribution, a metric $\mathcal{M}$ is introduced:

$$\mathcal{M} = \mathrm{F}(\theta) + \mathbf{1}, \tag{A.2}$$

with the Fisher Information Metric

$$\mathrm{F}(\theta) = \left\langle \frac{\partial \mathcal{H}(d \mid \xi)}{\partial \xi} \frac{\partial \mathcal{H}(d \mid \xi)}{\partial \xi^\dagger} \right\rangle_{(d|\xi=\theta)}.$$

A coordinate transformation $g(\xi)$ is desired through which the metric, Eq. (A.2), becomes particularly simple, specifically

$$\mathcal{M} \overset{!}{=} \left(\frac{\partial g}{\partial \xi}\right)^\dagger \mathbf{1} \left(\frac{\partial g}{\partial \xi}\right). \tag{A.3}$$

Frank et al. (2021) show that this transformation does not exist globally, but an expression that approximates the metric around an expansion $\bar{\xi}$ does:

$$g(\xi, \bar{\xi}) = \sqrt{\bar{\mathcal{M}}}^{-1}\left(\xi - \bar{\xi} + \left(\frac{\partial y}{\partial \xi}\bigg|_{\bar{\xi}}\right)^{\mathrm{T}} (y(\xi) - y(\bar{\xi}))\right) \tag{A.4}$$

where $\bar{\mathcal{M}}$ is the local metric at the expansion point. This formula depends on a function $y(\xi)$, which in turn is defined as a transformation through which the Fisher Information Metric becomes "diagonal" in this sense:

$$\mathrm{F}(\theta) \overset{!}{=} \left(\frac{\partial y}{\partial \xi}\right)^\dagger \mathbf{1} \left(\frac{\partial y}{\partial \xi}\right)\bigg|_{\xi=\theta}. \tag{A.5}$$

For a Gaussian likelihood, the Fisher Information Metric can be calculated as

$$\mathrm{F}(\theta) = \left(\frac{\partial s'}{\partial \xi}\right)^\dagger N^{-1} \left(\frac{\partial s'}{\partial \xi}\right)\bigg|_{\xi=\theta}, \tag{A.6}$$

where s' is the noiseless data, $s' := R(s(\xi))$. Finally, a comparison between Eq. (A.5) and Eq. (A.6) suggests

$$y = \sqrt{N^{-1}}\, s'.$$

Appendix B: Construction of reference fields

Fig. 6 shows the signal for the cosmological parameters (cf. Table B.1) found by the Planck Collaboration (2020) (s_{CMB}) and Scolnic et al. (2022) (s_{SN}). These fields are parametric flat ΛCDM models, i.e.

$$\frac{H(a)^2}{H_0^2} = \Omega_\Lambda + \Omega_m a^{-3}. \tag{B.1}$$

This corresponds to the signal (see Eq. 8) of

$$s(x) = \ln\left(\frac{3}{8\pi G} H_0^2 (1 + \Omega_m(e^{3x} - 1))\right). \tag{B.2}$$

The comparison of s_{CMB} and s_{SN} illustrates the impact of different H_0 values on the signal's shape and amplitude. The 1σ regions in Fig. 6 are calculated through Gaussian propagation of the errors in Table B.1 following to Eq. (B.2).

Table B.1: Adopted values of H_0 and Ω_m from Pantheon+SH0ES and Planck2018 cosmological results, used for constructing flat ΛCDM reference fields to compare with charm1 and charm2 reconstructions.

	Pantheon+SH0ES Scolnic et al. (2022)	**Planck2018** Planck Collaboration (2020)
$\hat{H}_0$	73.60 ± 1.1	67.36 ± 0.54
Ω_m	0.334 ± 0.018	0.3153 ± 0.0073

Appendix C: Note on converting charm1 signal fields

For a meaningful comparison of the reconstructions between charm1 and charm2, we need to make adjustments due to slightly different signal definitions.

We translate the charm1 signal field, denoted by $s_{\texttt{charm1, before}} := \ln(\rho/\rho_{c,0})$, to the corresponding charm2 signal field satisfying the new definitions Eq. (**??**) and Eq. (9) through

$$s_{\texttt{charm1, after}} = \ln(\rho_{c,0} e^{s_{\texttt{charm1, before}}}). \tag{C.1}$$

The original charm1 reconstruction used only the Union2.1 dataset, which, at that time, was the latest available.